

Interlayer Aharonov-Bohm interference in tilted magnetic fields in quasi-one-dimensional organic conductors

Benjamin K. Cooper and Victor M. Yakovenko

Condensed Matter Theory Center and Center for Superconductivity Research,
Department of Physics, University of Maryland, College Park, Maryland 20742-4111, USA
(Dated: **cond-mat/0509039**, 1 September 2005)

We present a unified geometrical interpretation of various magnetoresistance oscillations in quasi-one-dimensional organic conductors in terms of Aharonov-Bohm interference in interlayer electron tunneling. We visualize a two-parameter pattern of oscillations for generic magnetic field orientations and relate it to experiments. We propose to use an in-plane magnetic field perpendicular to the chains to probe the anion ordering gap in (TMTSF)₂ClO₄. When the field exceeds a threshold, interlayer tunneling between different branches of electron spectrum becomes possible.

PACS numbers: 74.70.Kn, 72.15.Gd, 73.21.Ac.

Introduction. Angular magnetoresistance oscillations (AMRO), where resistivity oscillates as a function of the magnetic field orientation, were discovered [1, 2] in the quasi-two-dimensional organic conductors of the (BEDT-TTF)₂X family [3]. Early theories of AMRO [4, 5, 6] were formulated in terms of semiclassical electron trajectories on a cylindrical Fermi surface. Then it was realized that AMRO exist already for two layers [7, 8, 9] and represent an Aharonov-Bohm interference effect in interlayer tunneling [10]. This theory of AMRO can be also applied to bilayers made of semiconductors [10].

Here we use the bilayer approach to study AMRO in the quasi-one-dimensional (Q1D) organic conductors, such as (TMTSF)₂X [3]. These materials consist of parallel chains, which form layers with the interlayer spacing d and the interchain spacing b , as shown in Fig. 1a. The in-plane tunneling amplitude between the chains, $t_b \sim 250$ K [11], is much greater than the inter-plane tunneling amplitude $t_c \sim 10$ K [3]. Thus, we treat interlayer tunneling as a perturbation and calculate interlayer conductivity σ_c between just two layers in the presence of a tilted magnetic field $\mathbf{B} = (B_x, B_y, B_z)$, as shown in Fig. 1a. This bilayer approach [8, 9] gives a simple unified picture of all types of angular oscillations observed in the Q1D conductors [11, 12, 13, 14] and is equivalent to other theories [15]. We present contour plots of σ_c as

a function of two ratios B_x/B_z and B_y/B_z for models with one or several interlayer tunneling amplitudes [16]. This visualization reveals agreement and disagreement between theory and experiment and helps to determine the electronic parameters of the Q1D materials.

We also propose to use an in-plane magnetic field to determine the anion ordering gap E_g in (TMTSF)₂ClO₄. In this material, a superstructure in the orientation of the ClO₄ anions doubles the lattice period in the y direction and folds the in-plane electron dispersion into two branches [3]. We show that, when B_y exceeds a threshold value related to E_g , interlayer tunneling between different branches becomes possible, and σ_c increases sharply.

The two-parameter pattern of AMRO in tilted magnetic fields. We consider electron tunneling between two Q1D layers (Fig. 1a). The in-plane electron dispersion is

$$\varepsilon(k_x, k_y) = \pm v_F k_x - 2t_b \cos(k_y b / \hbar), \quad (1)$$

where energy ε is measured from the Fermi energy, $\pm v_F$ are the Fermi velocities on the opposite sheets of the open Fermi surface, $\mathbf{k} = (k_x, k_y)$ is the in-plane momentum, and k_x is measured from the Fermi momentum. The inter-layer tunneling is described by the Hamiltonian

$$\hat{H}_\perp = t_c \int \hat{\psi}_2^\dagger(\mathbf{r}) \hat{\psi}_1(\mathbf{r}) e^{i\phi(\mathbf{r})} d^2r + \text{H.c.}, \quad (2)$$

$$\phi(\mathbf{r}) = \frac{ed}{\hbar c} A_z(\mathbf{r}), \quad A_z(\mathbf{r}) = B_x y - B_y x, \quad (3)$$

where $\mathbf{r} = (x, y)$, c is the speed of light, e is the electron charge, A_z is the vector potential, and $\hat{\psi}_{1,2}$ are the electron destruction operators in the layers 1 and 2. The gauge phase $\phi(\mathbf{r})$ is due to the in-plane magnetic field.

We treat the in-plane electron motion quasiclassically. For $B_z \neq 0$, electrons move in time t along sinusoidal trajectories [17], as shown in Fig. 1a,

$$x(t) = x_0 \pm v_F t, \quad y(t) = y_0 \mp \left(\frac{2t_b c}{e v_F B_z} \right) \sin(\omega_c t), \quad (4)$$

$$\omega_c = \frac{e b v_F B_z}{\hbar c}, \quad B'_x = \frac{B_x}{B_z} \frac{2t_b d}{\hbar v_F}, \quad B'_y = \frac{B_y}{B_z} \frac{d}{b}, \quad (5)$$

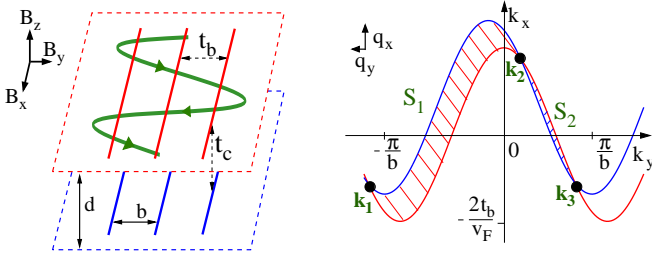


FIG. 1: (a) Geometry of electron in-plane motion and tunneling between two Q1D layers. (b) Fermi surfaces of the two layers shifted by the vector $\mathbf{q} = (ed/c)(B_y, -B_x)$.

where we also introduced the dimensionless variables B'_x and B'_y . The gauge phase (3) in Eq. (2) leads to interference between interlayer tunneling amplitudes $t_c e^{i\phi(\mathbf{r})}$ along the trajectory $\mathbf{r}(t)$. In Eq. (4), $y(t)$ oscillates with the period $\Delta t = 2\pi/\omega_c$, whereas $x(t)$ steadily increases, accumulating the phase $\Delta\phi = edB_y v_F \Delta t / \hbar c$ over one period. The average $\langle e^{i\phi(t)} \rangle_t$ vanishes unless $\Delta\phi = 2\pi n$, where n is an integer. This condition selects the Lebed magic angles $B'_y = n$ [12]. Using Eqs. (3), (4) and (5), we find the effective interlayer tunneling amplitude \tilde{t}_c

$$\tilde{t}_c = t_c \left\langle e^{i\phi(t)} \right\rangle_t = t_c J_n(B'_x) \quad \text{for } B'_y = n, \quad (6)$$

where J_n is the Bessel function.

Eq. (6) represents an interlayer Aharonov-Bohm effect. The condition $B'_y = n$ means that the flux of B_y through the area, formed by the interlayer distance d and the electron trajectory period $\Delta x = v_F \Delta t$, is $n\Phi_0$, where $\Phi_0 = hc/e$ is the flux quantum. Besides, \tilde{t}_c^2 (6) oscillates as a function of B'_x with the period $\Delta B'_x = \pi$, which represents the Danner-Kang-Chaikin (DKC) effect [11]. These oscillations are related to the flux of B_x through the area bounded by d and $\Delta y = 4t_b c / ev_F B_z$, the transverse width of the electron trajectory in Eq. (4). More precisely, it is necessary to consider the distance between the turning points of an electron trajectory viewed along the vector (B_x, B_y) . This will be discussed in more detail below from the momentum-space point of view.

The interlayer conductivity σ_c is given by a correlator of the interlayer tunneling events at times t and t' [8, 9]

$$\sigma_c \propto \text{Re} t_c^2 \left\langle \int_t^\infty e^{i\phi(t) - i\phi(t')} e^{-\frac{t'-t}{\tau}} dt' \right\rangle_t, \quad (7)$$

where τ is a relaxation time. Substituting Eqs. (3) and (4) in Eq. (7), we find, in agreement with Refs. [8, 9, 15],

$$\frac{\sigma_c(\mathbf{B})}{\sigma_c(0)} = \sum_{n=-\infty}^{\infty} \frac{J_n^2(B'_x)}{1 + (\omega_c \tau)^2 (n - B'_y)^2}. \quad (8)$$

In the limit $\omega_c \tau \rightarrow \infty$, only the term with $n = B'_y$ survives, and Eq. (8) reduces to $\sigma_c(\mathbf{B})/\sigma_c(0) = (\tilde{t}_c/t_c)^2$ with \tilde{t}_c from Eq. (6). In Fig. 2, we show the contour plot of $\sigma_c(\mathbf{B})/\sigma_c(0)$ vs. B'_x and B'_y calculated from Eq. (8) for $\omega_c \tau = \sqrt{50} \approx 7.1$. σ_c is maximal at the vertical stripes, labeled by an integer number, which correspond to the Lebed magic angles $B'_y = n$. Within the n -th vertical stripe, σ_c has alternating maxima and minima, indicated by circles and squares, which represent oscillations of J_n^2 vs. B'_x in Eqs. (6) and (8). Positions of these maxima and minima can be obtained from the Aharonov-Bohm interference in momentum space, as described below.

Eqs. (2) and (3) show that, in the process of interlayer tunneling, the in-plane electron momentum changes by

$$\mathbf{q} = (q_x, q_y) = (ed/c)(B_y, -B_x) \quad (9)$$

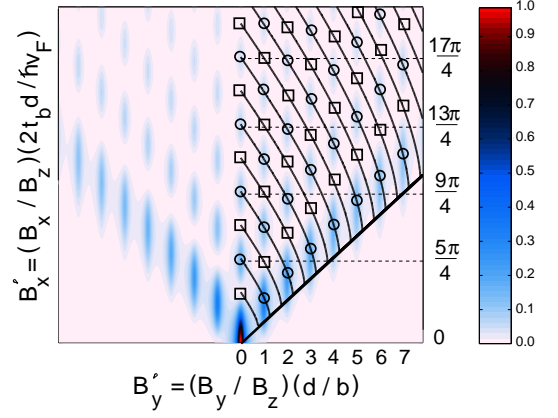


FIG. 2: Contour plot of the normalized interlayer conductivity $\sigma_c(\mathbf{B})/\sigma_c(0)$ vs. B'_x and B'_y calculated from Eq. (8).

Thus, the Fermi surfaces of the two layers are displaced relative to each other by the vector \mathbf{q} [8, 9], as shown in Fig. 1b. Electrons can tunnel between the layers only at the intersection points $\mathbf{k}_1, \mathbf{k}_2, \mathbf{k}_3$, etc. of the two Fermi surfaces, where the conservation laws of energy and momentum are satisfied. In the presence of B_z , a pair of trajectories connecting two intersection points has a phase difference proportional to the shaded momentum-space area $S_1 > 0$ or $S_2 < 0$ between the trajectories. The algebraic sum $S_1 + S_2 = q_x(2\pi\hbar/b)$ depends only on $q_x = (ed/c)B_y$. Constructive interference between \mathbf{k}_1 and \mathbf{k}_3 requires that $(S_1 + S_2)c/\hbar e B_z = 2\pi n$, which is equivalent to the Lebed condition $B'_y = n$.

Interference between \mathbf{k}_1 and \mathbf{k}_2 is controlled by the area S_1 . Introducing the dimensionless variable $S'_1 = S_1 c / \hbar e B_z$, we find from Fig. 1b

$$S'_1 = 2B'_x \sqrt{1 - \left(\frac{B'_y}{B'_x}\right)^2} + B'_y \left[\pi + 2 \arcsin \left(\frac{B'_y}{B'_x} \right) \right]. \quad (10)$$

Constructive interference requires that $S'_1 = 2\pi(j + 1/4)$, where j is an integer, and the extra phase $\pi/2$ appears because \mathbf{k}_1 and \mathbf{k}_2 are the extremal points on the Fermi surface, when viewed along the vector \mathbf{q} . The lines with circles show where in Fig. 2 this condition is satisfied. Maxima of σ_c are achieved at the circled intersections of these lines and the integer vertical lines, where both S_1 and $S_1 + S_2$ give constructive interference. These points correspond to the maxima of the Bessel functions in Eq. (8). The lines with squares in Fig. 2 show where the interference in S_1 is destructive (j is half-integer). At the intersections of these lines and the integer vertical lines, marked by squares, σ_c has minima, and the Bessel functions in Eq. (8) have zeros. Thus, $\sigma_c \rightarrow 0$ at $\omega_c \tau \rightarrow \infty$, and resistivity $\rho_c = 1/\sigma_c$ increases without saturation at the squares when $B \rightarrow \infty$, whereas $\rho_c(B)$ saturates at the circles [18]. The maxima and minima of σ_c create the checkerboard pattern of oscillations [15] in Fig. 2.

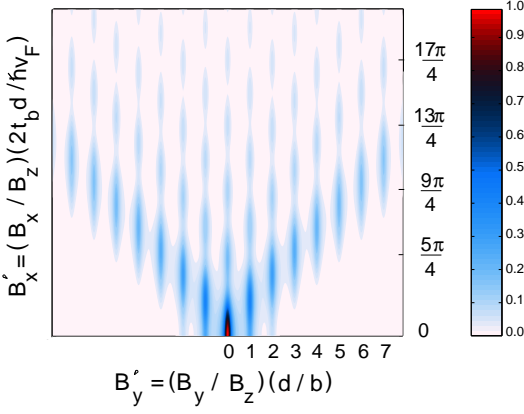


FIG. 3: Contour plot of the normalized interlayer conductivity $\sigma_c(\mathbf{B})/\sigma_c(0)$ vs. B'_x and B'_y calculated from Eq. (12).

The diagonal line $B'_x = B'_y$ in Fig. 2 corresponds to the third angular effect [13, 19]. At this line, the points \mathbf{k}_2 and \mathbf{k}_3 merge, and the area S_2 goes to zero in Fig. 1b. The checkerboard pattern of oscillations exists only for $|B'_x| > |B'_y|$ in Fig. 2. For $|B'_x| < |B'_y|$, the two Fermi surfaces do not cross in Fig. 1b, so interlayer electron tunneling is strongly suppressed. Thus, σ_c is very low and does not show any oscillations below the diagonal line in Fig. 2. This contradicts experiments [20], which show strong Lebed oscillations of σ_c vs. B'_y at $B_x = 0$.

To improve the theory, let us consider a model with interlayer tunneling amplitudes t_m between the chains shifted by m units in the y direction [16]. The tunneling displacement is $\mathbf{d} + m\mathbf{b}$, so the phase in Eq. (2) becomes

$$\phi(\mathbf{r}) = \frac{e}{\hbar c}(A_z d + A_y m b), \quad A_y = B_z x. \quad (11)$$

Comparing Eqs. (3) and (11), we see that results in this case can be obtained by substitution $B_y d \rightarrow B_y d - B_z m b$ and $B'_y \rightarrow B'_y - m$ in the old results. Eq. (6) transforms into $\tilde{t}_m = t_m J_{n-m}(B'_x)$ for $B'_y = n$, and Eq. (8) becomes

$$\frac{\sigma_c(\mathbf{B})}{\sigma_c(0)} = \sum_m \sum_{n=-\infty}^{\infty} \frac{t_m^2 J_{n-m}^2(B'_x)}{1 + (\omega_c \tau)^2 (n - B'_y)^2}, \quad (12)$$

where $t_m^2 = t_m^2 / \sum_l t_l^2$. The contour plot of Eq. (12) can be obtained by shifting the plot in Fig. 2 by m units along the B'_y axis and adding the shifted plots with the weights t_m^2 . The resulting contour plot, calculated for $t_0 = t_c$, $t_{\pm 1} = t_c/2$, and $t_{\pm 2} = t_c/4$, is shown in Fig. 3. At $B_x = 0$, $\sigma_c(B'_y)$ has maxima for those directions $B'_y = m$ where t_m exists [16]. Oscillations of σ_c vs. B'_x become smeared in Fig. 3, because the shifted maxima and minima of the checkerboard pattern in Fig. 2 add up out of phase. This is illustrated in Fig. 4, which shows that the DKC oscillations of $\sigma_c(B'_x)$ for $B_y = 0$ are much weaker for multiple t_m . Moreover, σ_c does not have zeros at $B'_y = n$: $\sigma_c(\mathbf{B})/\sigma_c(0) \rightarrow \sum_m \tilde{t}_m^2 / \sum_m t_m^2$ when $B \rightarrow \infty$.

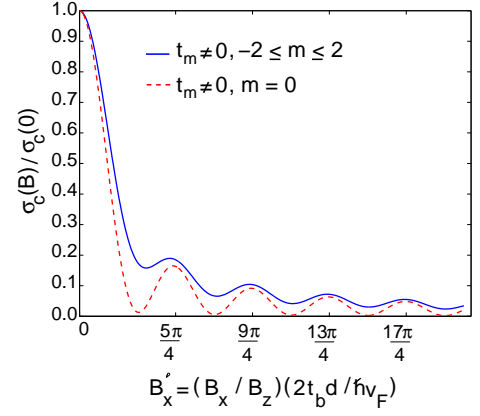


FIG. 4: Normalized interlayer conductivity $\sigma_c(\mathbf{B})/\sigma_c(0)$ vs. B'_x for $B_y = 0$ calculated from Eqs. (8) and (12).

Thus, $\rho_c(B)$ saturates on the integer lines in Fig. 3, but grows without saturation between the lines. Weak DKC oscillations of $\sigma_c(B'_x)$ at $B_y = 0$ and strong Lebed oscillations of $\sigma_c(B'_y)$ at $B_x = 0$ correspond qualitatively to (TMTSF)₂PF₆ [20, 21], indicating that several t_m are present. The opposite case, strong DKC and weak Lebed oscillations, is found in (TMTSF)₂ClO₄ [11, 22], suggesting that it has only one dominant $t_0 = t_c$ [23]. Quantitative comparison between the calculated plots and the experimental data for $\sigma_c(B'_x, B'_y)$ would help to identify the right models of AMRO in Q1D conductors.

Amplitudes t_m do not necessarily represent the overlaps between the Wannier wave functions on distant chains. They may be effective parameters in a model [24] where $\varepsilon(k_x)$ has curvature, and v_F depends on k_x in Eq. (1) and varies along the quasiclassical trajectory (4). The resulting expression for σ_c can be written in a form similar to Eq. (12) with some effective parameters t_m , which themselves may depend on \mathbf{B} [24].

Using an in-plane magnetic field to determine the anion gap in (TMTSF)₂ClO₄. In (TMTSF)₂ClO₄, the orientational superstructure of the inorganic anions ClO₄ doubles the lattice period in the y direction at 24 K [3]. As a result, the energies of the odd and even chains split by $\pm E_g$, which causes mixing of the states with momenta k_y and $k_y + \pi\hbar/b$. The in-plane electron dispersion folds into two branches, labeled by the index α ,

$$\varepsilon_\alpha(k_x, k_y) = v_F k_x - \alpha E_y(k_y), \quad \alpha = \pm \quad (13)$$

$$E_y(k_y) = \sqrt{E_g^2 + (2t_b)^2 \cos^2(k_y b / \hbar)}. \quad (14)$$

The Fermi surfaces are shown in Fig. 5a for $E_g/t_b = 0.1$.

When an in-plane magnetic field $(B_x, B_y, 0)$ is applied, the Fermi surface of one layer shifts by the vector \mathbf{q} (9) relative to another, as shown in Fig. 5a. Electrons can tunnel between the branches $\alpha, \beta = \pm$ only at the intersection points (k_x^*, k_y^*) determined by the equation

$$v_F q_x = \alpha E_y(k_y^* + q_y) - \beta E_y(k_y^*). \quad (15)$$

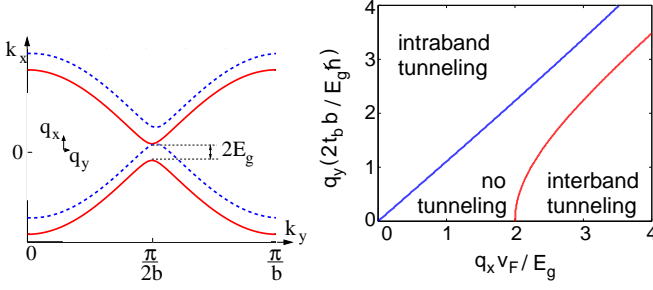


FIG. 5: (a) Fermi surfaces of two layers shifted by the vector (9). In each layer, the Fermi surface is split into two bands by the anion gap E_g . (b) Regions in the (q_x, q_y) space where different types of interlayer tunneling are possible or not.

Eq. (15) has solutions only in some regions of the (q_x, q_y) space, as shown in Fig. 5b. The boundaries of these regions are determined by the condition that the displaced Fermi surface touches the other one:

$$\alpha \frac{dE_y(k_y^* + q_y)}{dk_y} = \beta \frac{dE_y(k_y^*)}{dk_y}. \quad (16)$$

Solving Eq. (16) for k_y^* at a given q_y and substituting k_y^* into Eq. (15), we calculate q_x vs. q_y for the boundaries.

Interlayer tunneling within the same branch, $\alpha = \beta$, is possible above the diagonal line in Fig. 5b, which corresponds to the diagonal lines in Figs. 2 and 3 when $E_g \ll t_b$. If q_x exceeds the threshold

$$v_F q_x = B_y e d v_F / c \geq 2E_g, \quad (17)$$

interlayer tunneling between different branches, $\alpha = -\beta$, becomes possible. No interlayer tunneling is possible in the intermediate region in Fig. 5b, where the shifted Fermi surfaces do not cross in Fig. 5a. Thus, when \mathbf{B} is applied along the y axis, σ_c is strongly suppressed until B_y exceeds the threshold (17), and then σ_c increases sharply. Observation of this effect would be a strong confirmation the interlayer tunneling theory. The value of E_g can be determined from the measured threshold field B_y via Eq. (17). Strictly speaking, the interlayer tunneling amplitude involves a matrix element of the Hamiltonian (2), which contains the scalar product $\langle \psi_\alpha(k_y^* + q_y) | \psi_\beta(k_y^*) \rangle$. When $\alpha = -\beta$, the eigenfunctions are orthogonal for $q_y = 0$, so the matrix element vanishes. To get nonzero interlayer interbranch conductivity, some magnetic field B_x should be also applied, so that $q_y \neq 0$.

According to the measurements in Ref. [23], the Fermi velocity in $(\text{TMTSF})_2\text{ClO}_4$ is $v_F \approx 10^5$ m/s. Substituting this value and the interlayer distance $d = 1.35$ nm [3] into Eq. (17) and using the maximal stationary field of 45 T available at NHMFL in Tallahassee, we find the maximal anion gap $2E_g \approx 70$ K that can be probed with this method. Various estimates of E_g are reviewed in Ref. [25]. Refs. [26, 27] estimated E_g as $40 \div 50$ K, so the field of 45 T may be close to reaching the threshold (17) at

ambient pressure. The experiment can be also performed in pulsed fields or under pressure, where the anion superstructure is progressively suppressed [28]. This method can be also applied to $(\text{TMTSF})_2\text{ReO}_4$, where the anion superstructure doubles the lattice period in both y and z directions, and a rich pattern of AMRO is observed [29].

This work was supported by the NSF Grant DMR-0137726.

-
- [1] M. V. Kartsovnik *et al.*, JETP Lett. **48**, 541 (1988).
 - [2] K. Kajita *et al.*, Sol. St. Comm. **70**, 1189 (1989).
 - [3] T. Ishiguro, K. Yamaji, and G. Saito, *Organic Superconductors* (Springer, Berlin, 1998).
 - [4] K. Yamaji, J. Phys. Soc. Jpn. **58**, 1520 (1989).
 - [5] R. Yagi *et al.*, J. Phys. Soc. Jpn. **59**, 3069 (1990).
 - [6] M. V. Kartsovnik *et al.*, J. Phys. France I **2**, 89 (1992).
 - [7] Y. Kurihara, J. Phys. Soc. Jpn. **61**, 975 (1992); **62**, 255 (1993); D. Yoshioka, J. Phys. Soc. Jpn. **64**, 3168 (1992).
 - [8] R. H. McKenzie, P. Moses, Phys. Rev. Lett. **81**, 4492 (1998); Phys. Rev. B **60**, 7998 (1999); U. Lundin and R. H. McKenzie, *ibid.* **70**, 235122 (2004).
 - [9] T. Osada *et al.*, Physica E **12**, 272 (2002); **18**, 200 (2003); Synth. Metals **133–134**, 75 (2003); **135–136**, 653 (2003).
 - [10] V. M. Yakovenko and B. K. Cooper, cond-mat/0507120.
 - [11] G. Danner, W. Kang, and P. M. Chaikin, Phys. Rev. Lett. **72**, 3714 (1994).
 - [12] A. G. Lebed, JETP Letters **43**, 174 (1986).
 - [13] T. Osada, S. Kagoshima, and N. Miura, Phys. Rev. Lett. **77**, 5261 (1996).
 - [14] I. J. Lee and M. J. Naughton, Phys. Rev. B **57**, 7423 (1998).
 - [15] A. G. Lebed and M. J. Naughton, Phys. Rev. Lett. **91**, 187003 (2003).
 - [16] T. Osada, S. Kagoshima, and N. Miura, Phys. Rev. B **46**, 1812 (1992); E. I. Chashechkina and P. M. Chaikin, *ibid.* **65**, 012405 (2002).
 - [17] V. M. Yakovenko and H.-S. Goan, Phys. Rev. B **58**, 8002 (1998).
 - [18] A. G. Lebed, H.-I. Ha, and M. J. Naughton, Phys. Rev. B **71**, 132504 (2005); cond-mat/0503649.
 - [19] A. G. Lebed and N. N. Bagmet, Phys. Rev. B **55**, R8654 (1997).
 - [20] E. I. Chashechkina and P. M. Chaikin, Phys. Rev. Lett. **80**, 2181 (1998).
 - [21] G. M. Danner and P. M. Chaikin, Phys. Rev. Lett. **75**, 4690 (1995).
 - [22] T. Osada *et al.*, Phys. Rev. Lett. **66**, 1525 (1991); M. J. Naughton *et al.*, *ibid.* **67**, 3712 (1991).
 - [23] S. Takahashi *et al.*, Phys. Rev. B **72**, 024540 (2005).
 - [24] K. Maki, Phys. Rev. B **45**, 5111 (1992); A. G. Lebed, N. N. Bagmet, and M. J. Naughton, Phys. Rev. Lett. **93**, 157006 (2004).
 - [25] S. Haddad *et al.*, Phys. Rev. B **72**, 085104 (2005).
 - [26] S. Uji *et al.*, Phys. Rev. B **53**, 14399 (1996).
 - [27] H.-I. Ha, A. G. Lebed, M. J. Naughton, cond-mat/0503649.
 - [28] W. Kang, S. T. Hannahs, and P. M. Chaikin, Phys. Rev. Lett. **70**, 3091 (1993); H. Shinagawa *et al.*, Physica B **201**, 490 (1994); Synth. Met. **70**, 759 (1995); E. I. Chashechkina and P. M. Chaikin, Phys. Rev. B **56**, 13658 (1997).
 - [29] H. Kang *et al.*, Phys. Rev. B **68**, 132508 (2003).